Eur. Phys. J. E **12**, 69–76 (2003)
DOI 10.1140/epje/i2003-10028-4

THE EUROPEAN PHYSICAL JOURNAL E

Phase coexistence and dynamic properties of water in nanopores

I. Brovchenko[1,a], A. Geiger[1], A. Oleinikova[2], and D. Paschek[1]

[1] University of Dortmund, Physical Chemistry, Otto-Hahn-Str. 6, 44221 Dortmund, Germany
[2] Ruhr-Bochum University, Universitätsstr. 150, 44780 Bochum, Germany

Received 1 January 2003 /
Published online: 14 October 2003 –

Abstract. The dynamical properties of a confined fluid depend strongly on the (spatially varying) density. Its knowledge is therefore an important prerequisite for molecular-dynamics (MD) simulations and the analysis of experimental data. In a mixed Gibbs ensemble Monte Carlo (GEMC)/MD simulation approach we first apply the GEMC method to find possible phase states of water in hydrophilic and hydrophobic nanopores. The obtained phase diagrams evidence that a two-phase state is the most probable state of a fluid in incompletely filled pores in a wide range of temperature and level of pore filling. Pronounced variations of the average and local densities are observed. Subsequently, we apply constant-volume MD simulations to obtain water diffusion coefficients and to study their spatial variation along the pore radius. In general, water diffusivity slightly decreases in a hydrophilic pore and noticeably increases in a hydrophobic pore (up to about 40% with respect to the bulk value). In the range of gradual density variations the local diffusivity essentially follows the inverse density and the water binding energy. The diffusivity in the quasi–two-dimensional water layers near the hydrophilic wall decreases by 10 to 20% with respect to the bulk value. The average diffusivity of water in incompletely filled pore is discussed on the basis of the water diffusivities in the coexisting phases.

PACS. 61.20.Ja Computer simulation of liquid structure – 64.70.Fx Liquid-vapor transitions

1 Introduction

The molecular dynamics in fluids depends strongly on the local density, which may vary in space due to, for example, the presence of a solid substrate or of an interface between coexisting liquid and vapor phases. The influence of a surface on the properties of a fluid is especially complicated for fluids confined in narrow pores, where surface effects interplay with confinement effects.

The short-time translational self-diffusion of water in porous media at ambient temperature was studied by neutron scattering. The obtained self-diffusion coefficients D were found close to the bulk value (in a Vycor glass with an average pore radius $R_{\mathrm{P}} = 25\,\text{Å}$) [1], lower than the bulk value by about 24% (in Gelsil glass with $R_{\mathrm{P}} = 13\,\text{Å}$) [2] and lower than the bulk value by 26% and 40% (in siliceous MCM-41 with $R_{\mathrm{P}} = 14$ and $10\,\text{Å}$, respectively) [3]. The water diffusivity remains almost unchanged, when the level of pore filling is decreased to 25% in a Vycor glass [1], whereas in narrower pores D becomes lower by about 20%, when the level of pore filling is decreased to 5% [2]. The long-time translation diffusion coefficient of water in nanopores, measured by NMR, is many times lower than the bulk value [4,5]. A strong enhancement of the long-time diffusivity of water was found when decreasing the level of pore filling to less than 30% [6,7]. A similar effect is observed for subcritical fluids in zeolites [8].

There are numerous computer simulations of water diffusivity in pores [9–17]. Rather different changes of the average diffusion coefficient D due to the confinement were reported: from increase up to about 50% [9,13] to decrease of about 50% [14] with respect to the bulk value. Note also that the local diffusivity of water was found to increase [9,11,13] or to decrease [10–14] near a pore wall. Such a variety of water dynamics is caused not only by the use of various substrate structures, strengths of water-substrate interaction and pore sizes, but also by rather arbitrary imposed average water density in the pores. The latter factor prevents a systematic analysis of the available simulation results, especially in view of the strong density dependence of the water diffusivity [18]. The knowledge of the average fluid density in a pore at thermodynamic equilibrium is a necessary prerequisite for a correct simulation. This requires the knowledge of the fluid phase state in the pore. In the practically most important situation a confined fluid is in equilibrium with its saturated bulk fluid and exists in a vapour or in a liquid one-phase state. This corresponds to capillary evaporation or capillary

[a] e-mail: brov@heineken.chemie.uni-dortmund.de

condensation, respectively (see Ref. [19] as an example of such a simulation for water). An underestimation of the equilibrium density may result in a simulation of metastable or even unstable states, whereas its overestimation means that the confined liquid is in equilibrium with a bulk liquid at pressures higher than the saturation vapor pressure. In the closed pores, which are incompletely filled with a subcritical fluid, two-phase states may be expected in a wide range of pore filling. This means that simulations of fluids in incompletely filled pores require the knowledge of the coexistence curve of the fluids in the pores, *i.e.* the average densities of the coexisting phases at various temperatures. Imposing a one-phase state may result in simulations of non-equilibrium states. Recent simulations of the coexistence curves of water in nanopores show a rich phase behaviour and the dominance of two-phase states in wide density and temperature ranges [20,21].

In this paper we present simulations of the coexistence curves of water in cylindrical hydrophobic and hydrophilic nanopores with smooth walls. The obtained states are then used for the simulation of water diffusivity in the coexisting phases.

2 Phase behaviour of water in nanopores

TIP4P water [22] was simulated in cylindrical pores with radii $R_{\rm P} = 20\,$Å. The interaction between the water molecules and the substrate was described by a (9-3) Lennard-Jones (LJ) potential, which depends on the distance between the oxygen atoms and the wall only. The phase diagrams of the pore water, presented in this paper, were calculated for two well-depths U_0 of the LJ potential, $U_0 = -0.39$ kcal/mol and $U_0 = -4.62$ kcal/mol. These two strengths of water-substrate interaction represent strongly hydrophobic and strongly hydrophilic substrates, respectively. The water-water interactions were calculated by using a spherical cutoff with $r_{\rm C} = 12\,$Å. For further technical details see references [20] and [21].

The most direct method to observe the phase separation of a fluid in a pore is the method of temperature quench from a one-phase supercritical regime to subcritical temperature at various average fluid densities in the pore (level of pore filling) [23,24]. Snapshots of water molecules in the two pores under consideration at $T = 300$ K, obtained by a quench from a supercritical state at $T = 600$ K (the critical temperature of bulk TIP4P water is about 580 K [20]), are shown in Figure 1. Alternating domains of the two coexisting phases are clearly seen in both cases. In the hydrophilic pore (Fig. 1) the lower-density phase appears as two adsorbed water layers and vapour in the pore interior, whereas the higher-density coexisting phase contains liquid water in the pore interior in addition to the two water layers near the pore wall. In the hydrophobic pore (Fig. 1) there are no adsorbed layers on the pore wall, and a sequence of alternating domains of the coexisting vapor and liquid phases is observed. Despite the apparent simplicity and the possibility to observe the interface between the coexisting phases (see Fig. 1),

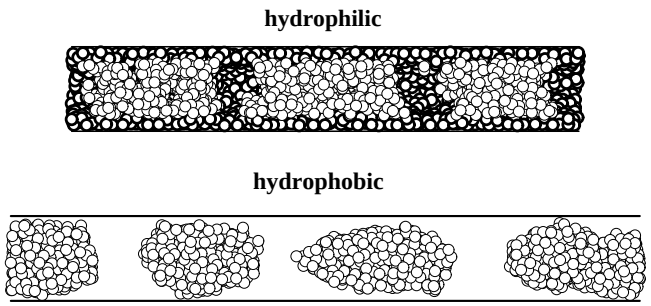

Fig. 1. Arrangement of water oxygens in hydrophilic and hydrophobic cylindrical pore with radius $R_{\rm P} = 20\,$Å at $T = 300$ K and with average densities 0.794 g/cm^3 and 0.369 g/cm^3, respectively. A bisection of the cylinders is shown in both cases. The water molecules near the wall of the hydrophilic pore (less than 7.5 Å) are indicated by darker circles.

the method of temperature quench is not widely used for the simulation of the properties of coexisting phases due to several reasons. First of all, the simulation of an equilibrated domain structure demands simulations of large systems (at least 10^3 to 10^4 molecules in the nanopores) in long pores (L about 10^2 $R_{\rm P}$) even at high temperatures, where the equilibrium length of the domains is comparably short (a few $R_{\rm P}$). At low temperatures close to the ambient one, the equilibrium length of the liquid domains essentially exceeds the pore lengths, which are accessible in simulations [24]. As a result, the properties obtained from short-pore simulations are distorted by the increased occurence of interfaces. So, the simulations presented in Fig. 1 could not be used for an accurate study of the properties of the coexisting phases.

In the present paper the densities of the coexisting phases of water in pores at various temperatures were obtained by Monte Carlo simulations in the Gibbs ensemble (GEMC) [25], where each phase is located in a separate cell, representing a cylindrical pore with periodic boundary condition along the pore axis. Equilibration of the chemical potentials of the two phases is achieved by numerous molecular transfers between the two simulation cells, whereas the equilibration of the pressure is provided by a volume exchange between the cells. Efficient techniques for the molecular transfers [19–21] allow us to simulate liquid-vapour coexistence of bulk water even at supercooled temperatures down to 125 K, while the coexistence between two dense and heterogeneous phases of water in hydrophilic pores may be simulated down to 250 K.

The obtained coexistence curves of water in both pores, which were studied, are shown in Figure 2. In the hydrophilic pore the layering transition, *i.e.* the quasi–two-dimensional liquid-vapor phase transition near the pore wall, occupies the low-density range up to about 0.4 g/cm^3. The liquid-vapor phase coexistence of the "inner" water, which occurs in the pore with a wall covered with two water layers, shown in Figure 1, is located in the range of average densities from about 0.6 to 1.0 g/cm^3 at ambient temperatures (Fig. 2). Density profiles for these two coexisting phases at two different temperatures are

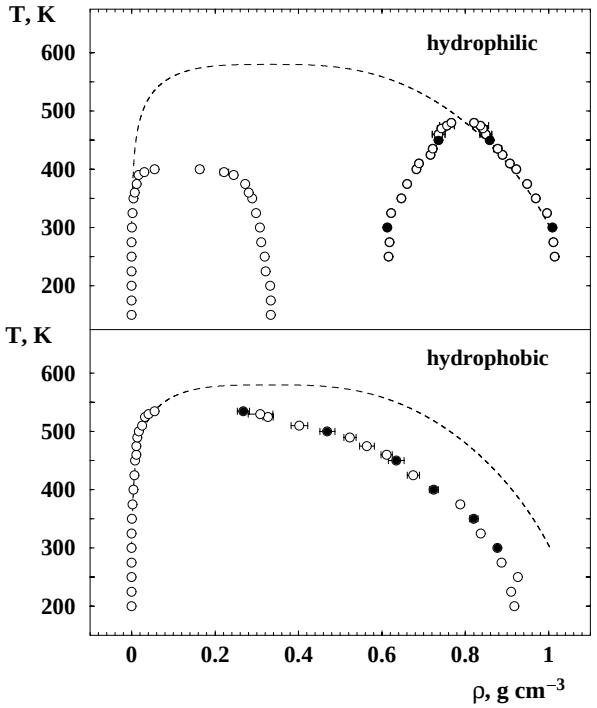

Fig. 2. Coexistence curves of water in the hydrophilic and hydrophobic cylindrical pores with radius $R_P = 20$ Å. The coexistence curve of bulk water for the same model is shown by the dashed line. Full circles indicate the systems used for the diffusivity study.

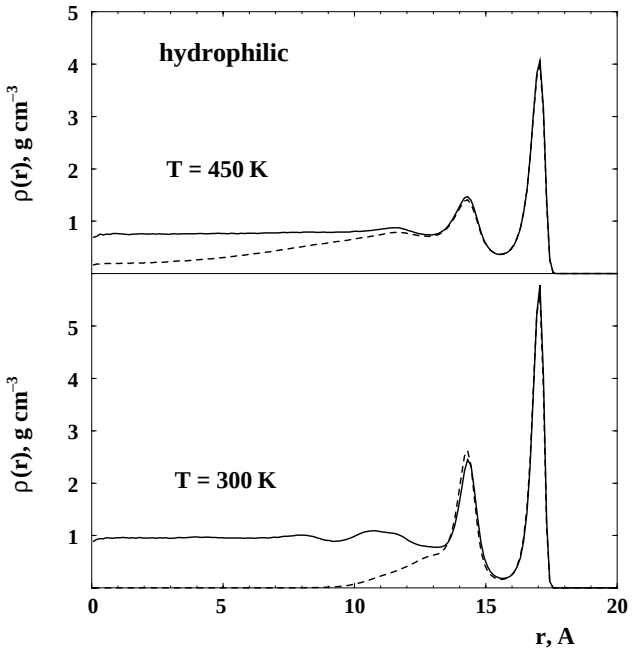

Fig. 3. Density profiles of the coexisting lower-density phase (dashed lines) and high-density phase (solid line) of water in the hydrophilic pore at two different temperatures.

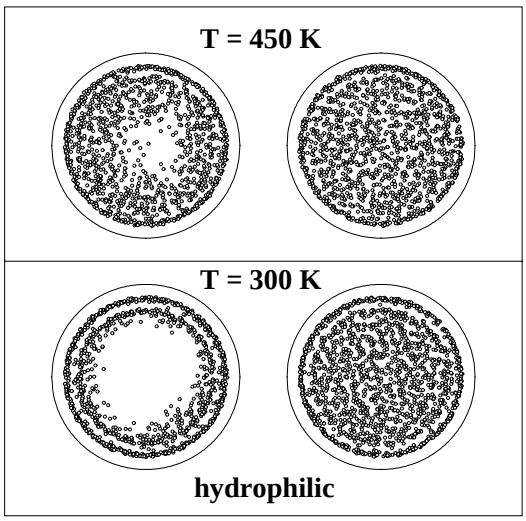

Fig. 4. Arrangement of water oxygens in coexisting phases in the hydrophilic pore; view along the axis of the cylindrical pore with radius $R_P = 20$ Å.

shown in Figure 3 and evidence that the structure of the two water layers near the pore wall is almost identical in both phases in a wide temperature range. In the pore interior liquid water becomes highly uniform at low temperatures (Fig. 3). The bottle-like shape of the liquid-vapor coexistence curve of the "inner" water, seen in Figure 2, originates from the formation of a wetting layer in the vapor phase when the temperature increases up to about 400–430 K. This is clearly seen from the density profiles in Figure 3 and from the snapshots of water molecules in the coexisting phases in Figure 4. Note also that the density of the liquid phase in the pore interior slightly decreases towards the pore axis at high temperatures.

In the hydrophobic pore there is a single liquid-vapor phase transition (see Fig. 2). The coexistence curve differs from the bulk mainly due to the decrease of the average density of the liquid phase. The density profiles in the liquid phase evidence a decreasing water density towards the pore wall and this effect becomes more pronounced with increasing temperature (see Figs. 5 and 6). Pronounced oscillations of the water density near the pore wall at $T = 300$ K weaken at higher temperatures.

Starting from the densities of the coexisting phases, which were obtained in the GEMC simulations, constant-volume MD simulations were performed next to study the dynamics of the water molecules in the pores.

3 Diffusion of water in nanopores

We determined the self-diffusion coefficients of the water molecules in hydrophilic and hydrophobic pores of 20 Å radius by molecular-dynamics (MD) simulations. The simulations were carried out for the two coexisting phases in the hydrophilic pores at 300 K and 450 K (see Fig. 3) as well as for the liquid phase in the hydrophobic pore at six different temperatures (shown in Fig. 5). For the MD simulations we employed the MOSCITO simulation program using a leapfrog integration scheme in combination

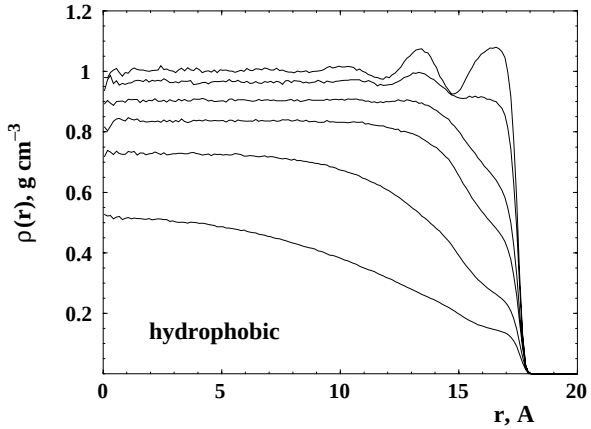

Fig. 5. Density profiles of the saturated liquid water in the hydrophobic pore at $T = 300$ K, 350 K, 400 K, 450 K, 500 K, and 535 K (from top to bottom).

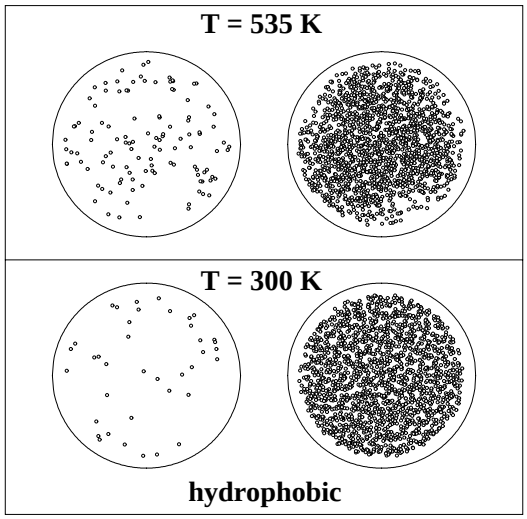

Fig. 6. Arrangement of water oxygens in coexisting phases in the hydrophobic pore; view along the axis of the cylindrical pore with radius $R_{\rm P} = 20$ Å.

with SHAKE for solving the constraint dynamics. The timestep 2 fs was chosen for all simulations. In order to be able to perform the simulations most efficiently we considered three-dimensional periodic boundary conditions. The long-range interactions were treated by smooth particle mesh Ewald summation [26] with a mesh size of approximately 1.2 Å. For the real space term and LJ interactions a cutoff radius of 9 Å has been used. In order to avoid problems due to the application of the minimum image convention we used a box size of 50 Å in x- and y-direction (perpendicular to the pore axis). The effect of the (artificial) periodicity introduced in x- and y-direction as well as of the different treatment of the long-range interactions has been studied by comparing the density profiles obtained by MD simulations and Gibbs ensemble technique. In all cases the data obtained by the different methods match very well. Each simulation consisted of an initial equilibration period of 0.5 ns and a subsequent production run of 2 ns which allow a sufficiently accurate determination of the dynamical properties. For the equilibration period as well as for the production run the temperature has been controlled by the Berendsen weak coupling [27] using $\tau_T = 2$ ps. The number of water molecules considered in the simulations varied between 1200 to 1700. The self-diffusion coefficients $D_{\rm bulk}$ of the bulk TIP4P water at various temperatures were simulated in the NPT ensemble at $P = 1$ bar. The obtained values of $D_{\rm bulk}$ and $\rho_{\rm bulk}$ are shown in Table 1. Note that the presented values of $\rho_{\rm bulk}$ within 2% agree with the densities of the bulk liquid phase obtained by GEMC simulations of the liquid-vapour coexistence curve [20].

Table 1. Self-diffusion coefficients D_z, D_{xy} and D (in 10^{-9} m^2/s) of water in a saturated liquid phase in the hydrophobic pores, in the low-density (phase 1) and high-density (phase 2) coexisting phases in the hydrophilic pores. Coefficients D_z were estimated both for the short-time intervals ($D_z^{\rm short}$), which were used for the estimation of the local coefficients (see text) and for the long-time interval 100–400 ps ($D_z^{\rm long}$). Coefficients D were obtained, based on the short-time diffusivities. $D_{\rm bulk}$ is the self-diffusion coefficient and $E_{\rm bulk}$ (in kcal/mol) is the water binding energy and $\rho_{\rm bulk}$ (in g/cm^3) is the density of bulk water at the corresponding temperatures.

T (K)	$D_z^{\rm short}$	$D_z^{\rm long}$	D_{xy}	D	$D_{\rm bulk}$	$E_{\rm bulk}$	$\rho_{\rm bulk}$
hydrophobic pore							
300	4.61	4.65	4.21	4.34	3.47	−20.06	0.99
350	9.83	9.88	8.04	8.63	7.49	−18.55	0.95
400	17.4	18.3	13.6	14.9	13.3	−17.28	0.90
450	26.3	27.8	20.8	22.6	20.8	−15.82	0.83
500	43.1	46.2	32.3	35.9	29.8	−14.19	0.73
535	67.8	81.8	55.7	59.7	43.0	−12.83	0.62
hydrophilic pore, phase 1							
300	3.93	3.52	2.48	2.96	3.47	−20.06	0.99
450	20.6	22.5	15.6	17.3	20.8	−15.82	0.83
hydrophilic pore, phase 2							
300	3.39	3.41	2.71	2.94	3.47	−20.06	0.99
450	18.0	19.7	14.4	15.6	20.8	−15.82	0.83

It is reasonable to consider two components of the total mean-square displacement (MSD) of water molecule in a cylindrical pore: the MSD along the pore axis $\langle \Delta z^2 \rangle$ and the MSD in the xy-plane $\langle \Delta (xy)^2 \rangle = (\langle \Delta x^2 \rangle + \langle \Delta y^2 \rangle)/2$, normal to the pore axis z. Due to the cylindrical geometry of the pore it is also useful to cosider two components of the in-plane MSD $\langle \Delta (xy)^2 \rangle$: the MSD along the pore radius $\langle \Delta r^2 \rangle$ and the tangential MSD $\langle \Delta s^2 \rangle$ along the direction pependicular to the radius vector in the xy-plane ("parallel to the pore wall"). In all cases the orientation of the corresponding vectors were defined from the initial position of the considered molecule. The time dependences of $\langle \Delta z^2 \rangle$ and $\langle \Delta (xy)^2 \rangle$ of the water molecules in the hydrophobic pore are shown in Figure 7. The MSD along the pore axis $\langle \Delta z^2 \rangle$ shows a linear time dependence for all considered temperatures, whereas $\langle \Delta (xy)^2 \rangle$ achieves a

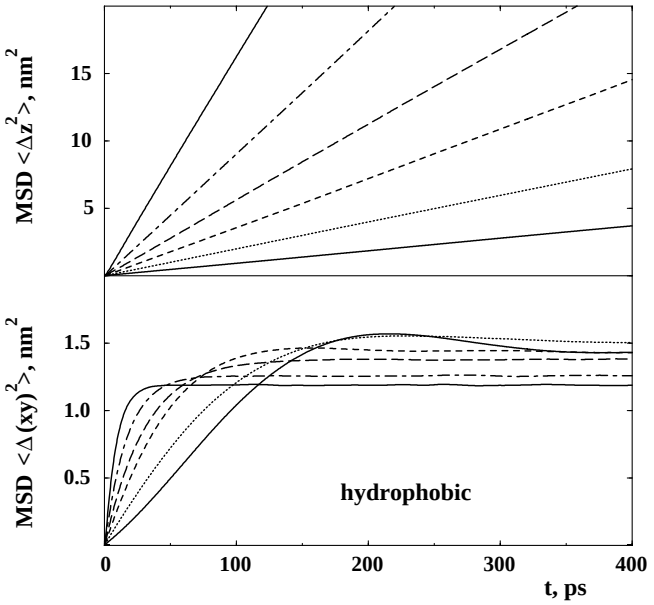

Fig. 7. Time dependences of the mean-square displacements $\langle \Delta z^2 \rangle$ and $\langle \Delta (xy)^2 \rangle$ in the hydrophobic pore (see text for details). The corresponding temperatures are 535 K (max $\langle \Delta z^2 \rangle$), 500 K, 450 K, 400 K, 350 K, 300 K (min $\langle \Delta z^2 \rangle$).

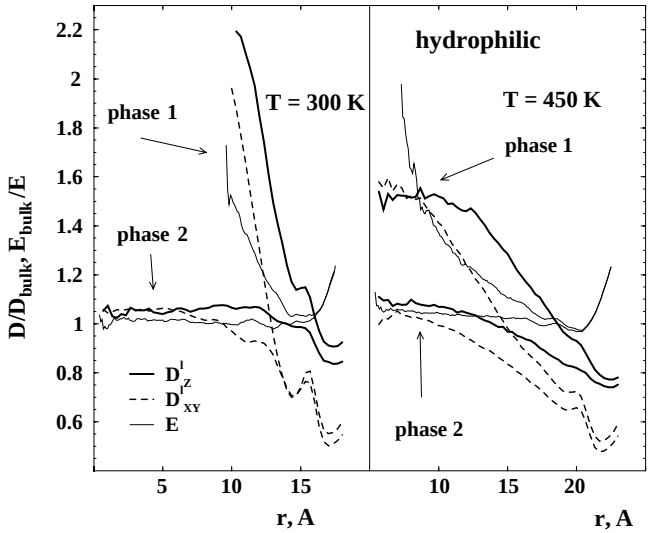

Fig. 8. Local self-diffusion coefficients $D_z^{\rm l}$ and $D_{xy}^{\rm l}$, normalized by the bulk diffusivity at the same temperature (see Tab. 1) in the coexisting low-density phase (phase 1) and high-density phase (phase 2) of water in the hydrophilic pore. Change of the normalized inverse water binding energy $E_{\rm bulk}/E_i$ is shown as function of the distance r from the pore axis.

plateau value with time due to the confining effect of the pore in these directions. Note that the plateau values of $\langle \Delta (xy)^2 \rangle$ decrease with temperature (Fig. 7) due to the non-uniform distribution of the water density along the pore axis (this effect was noted in Ref. [28]) and a narrowing of the mass distribution in the case of a hydrophobic pore (see density profiles in Fig. 5).

The self-diffusion coefficients of water D_z, D_{xy}, D_r, D_s were determined from the slopes of the time-dependent MSDs $\langle \Delta z^2 \rangle$, $\langle \Delta (xy)^2 \rangle$, $\langle \Delta r^2 \rangle$ and $\langle \Delta s^2 \rangle$, respectively. With the exception of D_z all other components become strongly time dependent due to the confinement. Therefore, only some initial time intervals (from 2 to 10 ps for $T = 300$, 400 K; from 1 to 5 ps for $T = 450$, 500 K and from 0.5 to 2.5 ps for $T = 535$ K) were used for the determination of the coefficients D_{xy}, D_r and D_s, which thus describe the short-time diffusion behaviour in the confining pore. (The obtained values of the self-diffusion coefficients D_z, D_{xy} and $D = (D_z + 2D_{xy})/3$ for all studied systems are shown in Tab. 1.) The described procedure in general yields diffusion coefficients for the diffusivity normal to the pore axis, which are smaller than D_z in the absence of any other structural effects [28–30]. These deviations are almost negligible (a few percents only) [29] in slit-like pores, whereas in a narrow cylindrical pore [30] strong confinement effect may prevent the determination of the diffusion coefficient from the slope of the MSD, because it becomes strongly non-linear already at very short times. In the latter case the diffusion coefficient in the plane normal to the pore axis may be estimated by solving the diffusion equation for a particle in a cylinder, assuming uniform density distribution. Using equation (3b) of reference [30], which gives the MSD in the xy-plane according to this assumption, we estimate the coefficients D_{xy} of the water in the hydrophobic pores at $T \geq 450$ K (at lower temperatures and in the case of a hydroplilic pore a strongly non-uniform density distribution along the pore radius makes it impossible). The values of D_{xy} obtained in such a way were found always higher than the values D_{xy}, obtained from the slope of the time dependence of $\langle \Delta (xy)^2 \rangle$ and close to the corresponding value of D_z (in agreement with the result of Ref. [30]).

In general, the water self-diffusion coefficient D_z increases in the hydrophobic pores up to 40% with respect to the bulk value, whereas in the hydrophilic pores it is very close to the bulk value (Tab. 1). An analysis of the average self-diffusion coefficients D is complicated by the systematic underestimation of the coefficients D_{xy} (see above), but we may conclude that the total water diffusivity noticeably increases in the hydrophobic pores, whereas in the hydrophilic pores it is only slightly depressed (if at all).

In order to study the spatial variation of the water diffusivity we calculated the local self-diffusion coefficients $D_z^{\rm l}$, $D_{xy}^{\rm l}$, $D_r^{\rm l}$ and $D_s^{\rm l}$ of the molecules, which start at time $t = 0$ at different distances r from the pore axis. All these coefficients were determined from the time dependence of the MSDs in the short-time intervals mentioned above. As Figure 8 shows, in the hydrophilic pore the local water self-diffusion coefficient $D_z^{\rm l}$ in the water layer near the pore wall is always about 10–20% below the bulk value. Weak oscillations in the water diffusivity near the pore wall reflect the layered water structure in this region (Fig. 3). As can be seen by comparing Figure 3 and Figure 8, the diffusivity of the "inner" water follows the inverse density. Figure 8 also shows the average binding energy $E_i = \Sigma U_{ij}$ of the water molecules as a function of the distance from the pore center; the sum extends over all neighbours j

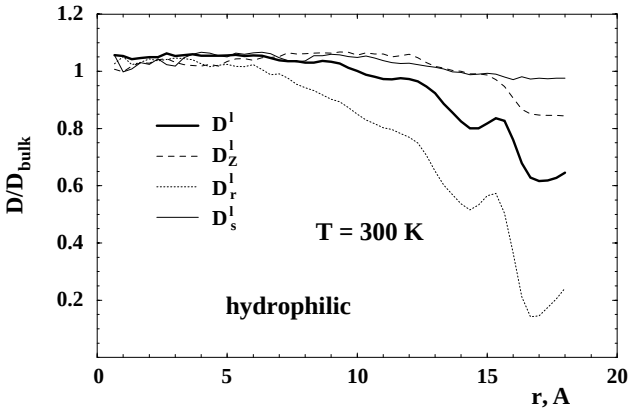

Fig. 9. Local self-diffusion coefficients $D^{\rm l}$, $D^{\rm l}_z$, $D^{\rm l}_r$ and $D^{\rm l}_s$ profiles, normalized by the bulk diffusivity at the same temperature (see Tab. 1) in the high-density phase of the hydrophilic pore.

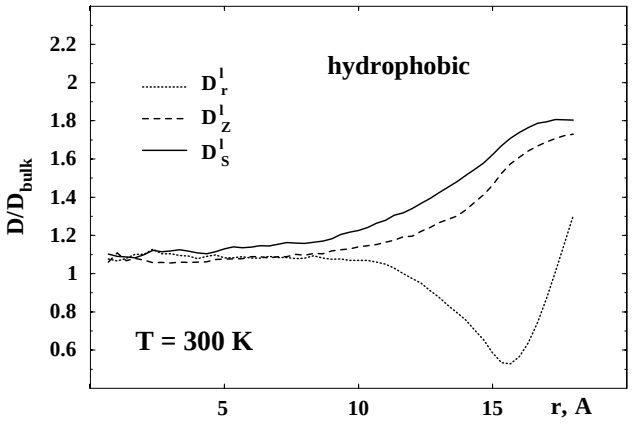

Fig. 11. Local self-diffusion coefficients $D^{\rm l}_z$, $D^{\rm l}_r$ and $D^{\rm l}_s$, normalized by the bulk diffusivity at the same temperature (see Tab. 1) in the liquid phase of water in the hydrophobic pore.

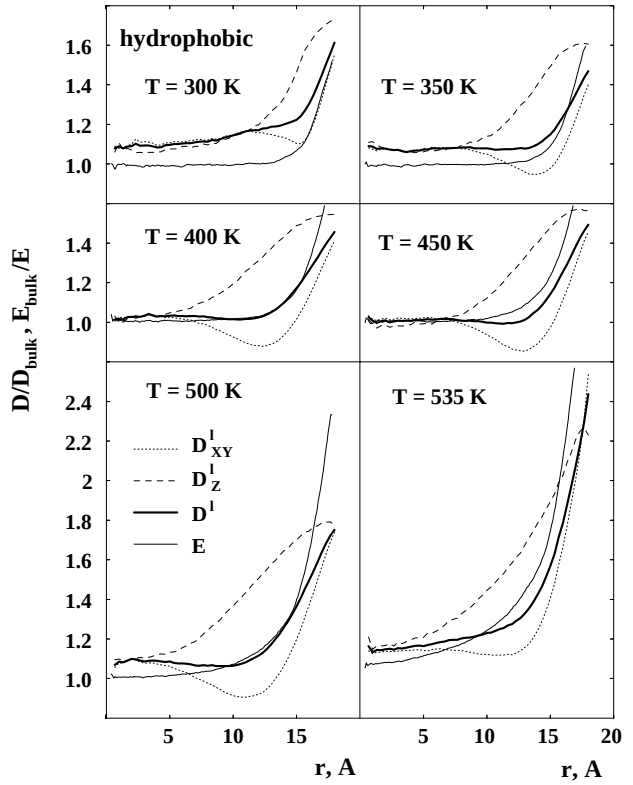

Fig. 10. Local self-diffusion coefficients $D^{\rm l}$, $D^{\rm l}_z$ and $D^{\rm l}_{xy}$, normalized by the bulk diffusivity at the same temperature (see Tab. 1) in the liquid phase of water in the hydrophobic pore. Change of the water binding energy E_i is shown as a function $E_{\rm bulk}/E_i$.

of the molecule i within the cutoff radius $r_{\rm C}$ [18]. In the pore interior, there is a clear correlation between diffusivity and binding energy, whereas near the pore wall the slowing-down influence of the pore wall is predominant. In Figure 9 the diffusion coefficients $D^{\rm l}$, $D^{\rm l}_z$, $D^{\rm l}_r$ and $D^{\rm l}_s$ in the liquid density phase are presented. Whereas the diffusion in the directions with no density variations ($D^{\rm l}_z$ and $D^{\rm l}_s$) are rather similar, the diffusivity along the pore radius ($D^{\rm l}_r$) changes by nearly a factor of 10, when approaching the wall. In the hydrophobic pore the local water diffusion coefficient $D^{\rm l}_z$ in the pore center in general is close to the bulk value at the same temperature and gradually increases (more than 50%) towards the pore wall (Fig. 10), showing a clear correlation with the profiles of the water binding energy (Fig. 10) and density (Fig. 5). $D^{\rm l}_z$ starts to increase deeply in the pore interior, where the water density is still uniform (Fig. 10). This reflects the fact that during the time interval, used for the estimation of $D^{\rm l}_z$, molecules change their position along the pore radius and thus may probe a large range of local densities. The self-diffusion coefficients $D^{\rm l}_z$ and $D^{\rm l}_{xy}$ are close to each other in the pore center and near the pore wall. Note that $D^{\rm l}_z$ monotonically increase towards the pore wall, while the $D^{\rm l}_{xy}$ show clear minima at a distance of a few molecular diameters from the pore wall. Figure 11 evidences that these minima originate exclusively from the MSD along the pore radius (see profiles of $D^{\rm l}_r$). Note also that the profile of the coefficient $D^{\rm l}_s$ is close to the profiles of the coefficient $D^{\rm l}_z$ at low temperatures (Fig. 11), but starts to deviate with increasing temperature (not shown).

4 Discussion

The obtained coexistence curves of water in nanopores clearly show that the two-phase state is the most probable state of water in a wide range of temperatures and average densities $\rho_{\rm av}$. The filling of a pore with a fluid is characterized by the level of pore filling $f = \rho_{\rm av}/\rho_0$, where ρ_0 is the fluid density in the completety filled pore. For hydrophilic pores, which show capillary condensation, usually ρ_0 is determined as the density of the liquid in the pore which is in equilibrium with a saturated bulk fluid. In a small cylindrical pore ($R_{\rm P} = 12\,$Å) the value of ρ_0 is about 20% higher than the density $\rho_{\rm l}$ of the liquid phase at the pore coexistence curve [19,20]. With increasing pore size $\rho_{\rm l}$ practically achieves the saturated bulk liquid density at a pore radius $R_{\rm P} = 20\,$Å ([21], see also Fig. 2).

Taking into account the same expected trend for ρ_0, use of the value ρ_l instead of ρ_0 may cause an overestimation of the value f by a few percents only. So, Figure 2 shows that at ambient temperature a two-phase state of water in a hydrophilic pore with radius 20 Å occurs at levels of pore filing $0\% < f < 40\%$ and $60\% < f < 100\%$, whereas a one-phase state occurs at $40\% < f < 60\%$. With increasing pore size the occurrence of a two-phase state becomes even more probable. Note also that in hydrophobic pores, which show capillary evaporation [19,20], two-phase states occupy the whole density region till ρ_l. This means that all properties of a fluid in an incompletely filled pore must be considered by taking into account a possible phase separation inside the porous medium both in the experiments and the simulations. For example, assuming the filling of a porous material with a fluid by a continuous growth of the thickness of its adsorbtion layer on the pore wall [1] may cause difficulties in the interpretation of experimental data [31]. In computer simulations, ignoring the liquid-vapour phase transitions of fluids in pores may result in simulations of non-equilibrium states. Experimentally observed capillary condensation in porous media, theoretical expectations for fluid phase behaviour in confinement and simulations of the fluid phase behaviour in pores evidence the phase separation scenario (for review see Ref. [32]). The strong influence of surface effects on the phase coexistence obtained in this work for fluids in simple cylindrical pores with smooth surfaces (Figs. 1–6) should be also expected for any porous media. The analysis of the additional effects of surface structuring and of pore disorder will need systematic studies of the liquid-vapour coexistence curves in such extremely complex systems.

We studied the dynamic properties of the most important dense water phases which occur in pores, neglecting the interface between coexisting phases. We found that the local diffusivity along the pore axis strongly correlates with the local density and the water binding energy, namely it increases with decreasing density and increasing energy. This trend is clearly seen in hydrophobic pores, where gradual changes of the water density along the pore radius are observed. The same trend may be noticed for water in the interior of hydrophilic pores, where only a slight variation of the density is observed and is reflected by the quite similar behaviour of the local coefficients D_z^l and D_s^l in the hydrophilic pore and in the hydrophobic pore at low temperatures, which both describe the MSDs along paths with equal density and energy.

The water diffusivity along the direction of the pore axis in the two specific layers near the wall of the hydrophilic pore deviates from this trend, insofar as the water binding energy weakens when approaching the pore wall (simply due to the effect of missing neighbours), but the water diffusivity decreases. This may be attributed to the strong orientational ordering of water molecules in these two layers (see Ref. [19] for the analysis of their structure). Note that the water diffusivity only slightly decreases near the hydrophilic surface (Fig. 8), where the water density strongly oscillates (Fig. 3). This shows that, in general, a varying binding energy has a stronger effect on the water dynamics near the surface than density variations due to the packing effect and corraborates with the results of reference [33] for the mobility of a polymer near the surface.

An analysis of the water diffusivity in the plane normal to the pore axis is complicated by the confining effect of the pore wall. The values of the coefficients D_{xy} and D obtained from the MSD over a finite-time interval (Tab. 1) may noticeably underestimate the limiting values for unrestricted short time diffusion. We expect, that the coefficients D_{xy}, obtained by a more appropriate method (wich must take into account both confining effect of a wall as described in Refs. [28–30], but also the non-uniform density distribution of the liquid in the pore), will be close to the coefficients D_z.

The profiles of the local coefficients D_r^l of the water in the hydrophobic pores show minima at some distance from the pore wall. Such a behaviour is typical for the diffusion normal to a reflecting wall, where the distance of such a minimum from the pore wall changes with the diffusion coefficient D and time of observation Δt as $(D\Delta t)^{0.5}$. The convergence of the values of D_z^l and D_r^l in the pore interior and near the pore wall (Fig. 10) strongly indicates that the water diffusivities along and normal to the pore axis are in close agreement.

In the hydrophilic pores the local coefficient D_r^l strongly decreases towards the pore wall (Fig. 9), showing a behaviour, which is typical for the diffusion normal to an adsorbing wall. So, considering short diffusion time intervals, when the MSD along the pore radius does not exceed R_P, we observe two kinds of water mobility in the radial direction. In hydrophilic pores (with adsorbing walls) the most immobilized molecules are located on the pore wall. In hydrophobic pores (with reflecting walls) the most immobilized water molecules are located at some distance from the pore wall.

Knowing the dynamic properties and the density of water in coexisting phases we can predict these properties in incompletely filled pores at any level of pore filling, neglecting the presence of fluid-fluid interfaces, whose concentration is extremely small at low temperatures [24]. In the case of liquid-vapour coexistence in a hydrophilic pore with a wall covered by two water layers the average diffusion coefficient should change slightly and almost linearly (due to the close densities of the phases), when the level of pore filling changes from 100% to about 60%. It is natural to expect a much stronger decrease of the water diffusivity near a structured surface (see, for example, Refs. [14,15, 17] in comparison with the smooth surfaces, considered in our study. In such a case diffusivities of the coexisting phases should differ much stronger and the total diffusivity should noticeably decreases with lowering f.

In hydrophobic and moderately hydrophilic pores the low-density coexisting phase is a vapour, which does not form liquid layer(s) on the pore wall [20,21]. The diffusivity in this phase is several orders of magnitude higher than in the liquid phase. The average diffusivity changes with f in a qualitatively different way, than in strongly hydrophilic pores: it always increases with lowering f due

to the increasing fraction of pore molecules in the vapour phase. For example, in a hydrophobic pore at 300 K we estimated the average diffusivity to increase by a factor of two when f decreases from 100% to about 30% (assuming the diffusivity in the vapour 10^4 times higher than in the liquid). The same trend may be expected in large hydrophilic pores, when the fraction of molecules in the adsorbed layer(s) becomes negligible. Note that experimental methods, which do not probe the diffusivities of molecules in the liquid and the vapour phases simultaneously, the measured diffusivity will not depend on f.

The effect of the interfaces between the domains of the coexisting phases should be taken into account at high temperatures, when the concentration of the interfaces increases and the equilibrium domain length decreases. Its influence on the diffusivity is not clear *a priori* and needs special studies.

This work was supported by Ministerium für Schule und Weiterbildung, Wissenschaft und Forschung des Landes Nordrhein-Westfalen and by DFG-Forschegruppe 436.

References

1. M.-C. Belissent-Funel, S.H. Chen, J.-M. Zanotti, Phys. Rev. E **51**, 4558 (1995).
2. V. Crupi, S. Magazu, D.Majolino, P. Migliardo, V. Venuti, M.-C. Bellissent-Funel, J. Phys. Condens. Matter **12**, 3625 (2000); V. Crupi, D. Majolino, P. Migliardo, V. Venuti, J. Phys. Chem. B **106**, 10884 (2002).
3. S. Takahara, M. Nakano, S. Kittaka, Y. Kuroda, T. Mora, H. Hamano, T. Yamaguchi, J. Phys. Chem. B **103**, 5814 (1999).
4. E.W. Hansen, R. Schmidt, M. Stocker, D. Akporiaye, Microporous Mater. **5**, 143 (1995).
5. R. Kimmich, S. Stapf, A.I. Maklakov, V.D. Skirda, E.V. Khozina, Magn. Reson. Imaging **14**, 793 (1996).
6. F. D'Orazio, S. Bhattacharja, W.P. Halperin, R. Gerhardt, Phys. Rev. Lett. **63**, 43 (1989).
7. F. D'Orazio, S. Bhattacharja, W.P. Halperin, R. Gerhardt, Phys. Rev. B **42**, 6503 (1990).
8. S.M. Auerbach, Int. Rev. Phys. Chem. **19**, 155 (2000).
9. R. Sonnenschein, K. Heinzinger, Chem. Phys. Lett. **102**, 550 (1983).
10. G. Barabino, C. Gavotti, M. Marchesi, Chem. Phys. Lett. **104**, 478 (1984).
11. S.H. Lee, P.J. Rossky, J. Chem. Phys. **100**, 3334 (1994).
12. J.J. Lopez Cascales, H.J.C. Berendsen, J. Garcia de la Torre, J. Phys. Chem. **100**, 8621 (1996).
13. C. Harting, W. Witschel, E. Spohr, J. Phys. Chem. B **102**, 1241 (1998).
14. E. Spohr, C. Hartnig, P. Gallo, M. Rovere, J. Mol. Liquids **80**, 165 (1999).
15. P. Gallo, M. Rovere, E. Spohr, J. Chem. Phys. **113**, 11324 (2000).
16. J. Martiand, M.C. Gordillo, Phys. Rev. B **64**, 021504 (2001).
17. P. Gallo, M. Rapinesi, M. Rovere, J. Chem. Phys. **117**, 369 (2002).
18. F. Sciortino, A. Geiger, H.E. Stanley, J. Chem. Phys. **96**, 3857 (1992).
19. I. Brovchenko, D. Paschek, A. Geiger, J. Chem. Phys. **115**, 5026 (2000); I. Brovchenko, A. Geiger, D. Paschek, Fluid Phase Eq. **183-184**, 331 (2001); I. Brovchenko, A. Geiger, J. Mol. Liq. **96-97**, 195 (2002).
20. I. Brovchenko, A. Geiger, A. Oleinikova, Phys. Chem. Chem. Phys. **3**, 1567 (2001); in *New Kinds of Phase Transitions: Transformations in Disordered Substances* (Kluwer Academic Publishers, 2002) p. 367.
21. I. Brovchenko, A. Geiger, A. Oleinikova, submitted to J. Chem. Phys.
22. W.L. Jorgensen, J. Chandrasekhar, J.D. Madura, J. Chem. Phys. **79**, 926 (1983).
23. B.K. Peterson, K.E. Gubbins, G.S. Heffelfinger, U. Marini Bettolo Marconi, F. Swol, J. Chem. Phys. **88**, 6487 (1988).
24. L.D. Gelb, K.E. Gubbins, Phys. Rev. E **55**, (1997) R1290; **56**, 3185 (1997).
25. A.Z. Panagiotopoulos, Mol. Phys. **62**, 701 (1987); **61**, 813 (1987).
26. U. Essmann, L. Perera, M.L. Berkowitz, T.A. Darden, H. Lee, L.G. Pedersen, J. Chem. Phys. **103**, 8577 (1995).
27. H.J.C. Berendsen, J.P.M. Postma, W.F. van Gunsteren, A. DiNola, J.R. Haak, J. Chem. Phys. **81**, 3684 (1984).
28. M.P. Allen, A.J. Masters, Mol. Phys. **79**, 435 (1993).
29. M. Schoen, J.H. Cushman, D.J. Diestler, C.L. Rhykerd jr., J. Chem. Phys. **88**, 1394 (1988).
30. A. Brodka, Mol. Phys. **82**, 1075 (1994).
31. J. Dore, Chem. Phys. **258**, 327 (2000).
32. L.D. Gelb, K.E. Gubbins, R. Radhakrishnan, M. Sliwinska-Bartkowiak, Rep. Prog. Phys. **62**, 1573 (1999).
33. F. Varnik, J. Baschnagel, K. Binder, Phys. Rev. E **65**, 021507 (2002).